Inter-impurity interaction and structure of a trapped bipolaron in doped conjugated polymers

1991 J. Phys.: Condens. Matter 3 8855

(http://iopscience.iop.org/0953-8984/3/45/008)

J. Phys.: Condens. Matter 3 (1991) 8855–8868. Printed in the UK

Inter-impurity interaction and structure of a trapped bipolaron in doped conjugated polymers

Kikuo Harigaya†
Department of Physics, Faculty of Science, University of Tokyo, Hongo 7-3-1, Bunkyo-ku, Tokyo 113, Japan

Received 25 March 1991

Abstract. The effects of an inter-impurity interaction are studied by the extended Peierls–Hubbard model. The Coulomb interactions in the chain are treated by the Hartree–Fock approximation. There are two acceptor-type impurities expressed by long-ranged Coulomb potentials with anisotropic dielectric constants. Stationary positions of the impurities as well as stationary lattice configurations and electronic wave functions are numerically determined self-consistently. Trapping of a bipolaron around impurities is found. The distance between impurities is of the order of the coherence length. Two mid-gap levels, which would exist for a free bipolaron, move to higher energies due to the strong dopant potential. The Coulomb interactions in the chain effectively weaken the strength of the dopant potential. The energy levels shift to lower energies with increasing interaction strengths. Dynamical conductivity (optical absorption) is calculated. The isolated peak in the lower frequencies is associated with the position of the localized level in the energy gap. The consequences for experimental observation of the impurity clustering are discussed.

1. Introduction

Doping of conjugated polymers, such as polyacetylene films, gives rise to dramatic changes in their physical properties. They are measured in thermodynamic experiments, transport, optical measurements, and so on. Some of the mechanisms remain unresolved. Therefore, the effect of doping on conjugated polymers is an important and quite interesting problem to be investigated.

In the preceding investigations [1–9], we have assumed a random distribution of impurities and investigated the electronic structures of doped conjugated polymers. When the impurities are charged impurities (dopants which released or accepted electrons in order to make a closed shell), we have assumed that the dopant configurations are disordered in the polymer chain direction and relied upon models with complete disorder. However, even if there is a strong possibility that the models with disorder simulate doped systems well, interactions would operate among the dopants in real materials. As a fairly large void would be present around dopants, the interactions might give rise to a more or less correlated distribution which some experiments indicate [10].

† Present address: Fundamental Physics Section, Physical Science Division, Electrotechnical Laboratory, Umezono 1-1-4, Tsukuba, Ibaraki 305, Japan.

0953-8984/91/458855 + 14 $03.50

This work, which incorporates the inter-impurity interactions, would be desirable for a more complete description of the metal–insulator transition.

In order to investigate further in this direction, we would require detailed knowledge about the effects of the inter-impurity interactions. We would like to know how the impurity configurations are changed as a result of the mutual interactions and thus how the electronic properties vary. Detailed investigation of this problem has been absent so far.

Quite recently, Cohen and Glick [11] have included the Hubbard Coulomb term and inter-impurity interactions in the Su–Schrieffer–Heeger (SSH) model [12]. The number of dopants is two or four, and they are modelled by ring charges. They determined stationary configurations of impurities as well as stationary lattice patterns, and have found impurity clustering due to the interactions. Furthermore, they have investigated the phonon dynamics around the soliton. However, an extensive knowledge of the impurity distribution and electronic structures has not yet been reported. Thus, it becomes necessary to carry out further investigations.

The purpose of the present paper is to study how the dopant configurations, lattice patterns, and electronic structures change due to the inter-impurity interactions.

For the chain system, we make use of the extended Peierls–Hubbard model [10], where the on-site and nearest-neighbour Coulomb interaction terms are taken into account in the SSH model [12]. The short-ranged Coulomb interactions assume effective screening of the Coulomb force among π-electrons. The interaction strength would become exponentially weaker if electrons separate further. We assume that the interactions are limited to electrons only on one site or on nearest-neighbour sites.

We consider two acceptor-type dopant ions. Each dopant is assumed to be a point charge. Mutual interaction between them is the long-range Coulomb force with a dielectric constant observed over the whole sample. Due to the large void, which would be present among dopants, the Coulomb potential would not be completely screened and a long-range component would remain. Therefore, the long-range Coulomb potential is assumed for the dopant potential, in contrast to short-range ones between electrons.

Interactions between the chain and dopants are also long ranged. The assumption would be appropriate because of the void. Though there might be some possible forms for realistic Coulomb potentials, we consider particularly the one used by Conwell and Jeyadev [13]. The same potential has been used in [9]. The dielectric constants are anisotropic depending on whether the direction of each component is parallel or perpendicular to the chain. The component in the chain direction is larger because π-electrons can move only in this direction. The dielectric constants might be locally different near the impurities. Thus the forms of the potentials around the impurities are different from those in regions far from them. However, we assume the same form as in [9] because the effects of the long-range tails of the impurity potentials are expected to be qualitatively independent of the details of the potential models. The Coulomb potential of the dopants generates a repulsive potential to the electrons in the chain. The π-electron density becomes smaller around dopants and an effective positive charge appears. Therefore, dopant and chain systems interact strongly. This interaction gives rise to trapping of a charged soliton around a dopant.

Furthermore, various assumptions and approximations are used throughout the paper. We assume that the dopants can move freely in a line parallel to the chain. Motion of the dopants around the chain is not considered. This assumption might simulate the finding that dopant columns and chains would be crystallinely ordered in highly oriented polyacetylene [14]. We use the Hartree–Fock approximation (HF) for the Coulomb

terms of the chain. This approximation would be valid enough because the coherence length is about eight lattice constants and can be regarded as large. We determine numerically the stationary dopant distribution and lattice patterns. Dopant positions and lattice displacements are used as order parameters as well as the HF variables.

Numerical results are reported in the following way.

First, we show the relative separation of dopants as a function of the Coulomb strengths of the chain. This depends sensitively on the nearest-neighbour Coulomb strength. The magnitude is of the order of the coherence length and increases as the strength increases. It depends weakly on the on-site strength.

Second, a typical configuration of the lattice and the electron density distribution are shown. We find a trapped bipolaron around dopants. This is an unstable excitation in the impurity-free chain. It is formed by balancing the attractive forces between solitons and dopants, and the repulsive forces between solitons and between dopants.

Next, we show the electronic level structures. We find that the characteristic structure of a bipolaron in the impurity-free system is absent. The positions of two mid-gap levels are shifted into the conduction band by the strong dopant potentials. As the Coulomb strengths increase, a new level splits off from the conduction band, or the localized level in the gap comes closer to the valence band. This is because the Coulomb interactions effectively weaken the dopant potential.

Finally, we calculate the dynamical conductivity (optical absorption) in order to look at how the change would be observed in the frequency dependence. There is a localized peak in the lower frequency region than that of the main inter-band transition peak. The position of the localized peak moves in association with the variation in electronic structure.

This paper is arranged as follows. In section 2, we present the model and explain the numerical method. In section 3, we report stationary configurations of the dopants, lattice patterns, and electron density. In section 4, we show the electronic level structure and calculate the dynamical conductivity. We summarize and discuss the paper in section 5.

2. Model and numerical method

We consider the following model

$$H = H_{\text{chain}} + H_{\text{dopant}}. \tag{2.1}$$

The first term is the extended Peierls–Hubbard model [10],

$$\begin{aligned} H_{\text{chain}} = &- \sum_{n,s} [t_0 - \alpha(u_{n+1} - u_n)](c^{\dagger}_{n+1,s} c_{n,s} + \text{HC}) \\ &+ U \sum_n c^{\dagger}_{n,\uparrow} c_{n,\uparrow} c^{\dagger}_{n,\downarrow} c_{n,\downarrow} + V \sum_n \left(\sum_s c^{\dagger}_{n,s} c_{n,s} \right) \left(\sum_{s'} c^{\dagger}_{n+1,s'} c_{n+1,s'} \right) \\ &+ \tfrac{1}{2} K \sum_n (u_{n+1} - u_n)^2 \end{aligned} \tag{2.2}$$

where t_0 is the hopping integral of the undimerized chain, α the electron–phonon coupling constant, u_n the displacement of the nth (CH)-unit, $c_{n,s}$ the annihilation operator of an electron at the nth site with spin s ($s = \uparrow, \downarrow$), U the on-site Coulomb repulsion strength, V the Coulomb strength between the nearest-neighbour sites, and K the spring

constant between the adjacent units. The second term of (2.1) is the contribution from the dopant ions modelled by point charges. The form is

$$H_{\text{dopant}} = \sum_{i \neq j} e^2/\varepsilon_\perp |x_i - x_j| + \sum_{n,s} V_n c^\dagger_{n,s} c_{n,s} \tag{2.3}$$

and

$$V_n = \sum_i e^2/\varepsilon_\perp [(na - x_i)^2 + (\varepsilon_\parallel/\varepsilon_\perp) d^2]^{1/2} \tag{2.4}$$

where e is the magnitude of the unit charge, $\varepsilon_\perp$ and $\varepsilon_\parallel$ the dielectric constants perpendicular and parallel to the chain, respectively, x_i the position of the centre of the ith dopant (it is a continuous variable), a the lattice constant of the undimerized system, and d the distance between the dopant ion and the chain. A possible screening mechanism is included in the anisotropic dielectric constants. The component parallel to the chain is larger than that perpendicular to it. Therefore, the magnitude of the bare charge is used for e. Possible local variations of dielectric constants are not considered. Effects of long-range potentials would not change so much, even if they are included. The first term of (2.3) is the Coulomb force between the dopants. We assume, for simplicity, that the dopants move in a line parallel to the chain. In highly oriented polyacetylene, the dopant columns and chains would be crystallinely ordered [14]. Motion of the dopants around the chain would be suppressed and motion in the chain direction would be dominant. The above assumption takes account of this situation. The second term of (2.3) represents the effects of the dopant potential on electronic systems. The same form has been used in [9]. The notions of short- and long-range Coulomb potentials have been summarized in section 1.

Using the Hartree–Fock approximation (HF), the U and V terms in (2.2) are replaced as follows:

$$c^\dagger_{n,\uparrow} c_{n,\uparrow} c^\dagger_{n,\downarrow} c_{n,\downarrow} \Rightarrow \langle c^\dagger_{n,\uparrow} c_{n,\uparrow} \rangle c^\dagger_{n,\downarrow} c_{n,\downarrow} + c^\dagger_{n,\uparrow} c_{n,\uparrow} \langle c^\dagger_{n,\downarrow} c_{n,\downarrow} \rangle - \langle c^\dagger_{n,\uparrow} c_{n,\uparrow} \rangle \langle c^\dagger_{n,\downarrow} c_{n\downarrow} \rangle \tag{2.5}$$

and

$$\begin{aligned}\Big(\sum_s c^\dagger_{n,s} c_{n,s}\Big)\Big(\sum_{s'} c^\dagger_{n+1,s'} c_{n+1,s'}\Big) &\Rightarrow \sum_{s,s'} [(\langle c^\dagger_{n,s} c_{n,s} \rangle c^\dagger_{n+1,s'} c_{n+1,s'} + c^\dagger_{n,s} c_{n,s} \langle c^\dagger_{n+1,s'} c_{n+1,s'} \rangle - \langle c^\dagger_{n,s} c_{n,s} \rangle \langle c^\dagger_{n+1,s'} c_{n+1,s'} \rangle) \\ &- (\langle c^\dagger_{n,s} c_{n+1,s'} \rangle c^\dagger_{n+1,s'} c_{n,s} + c^\dagger_{n,s} c_{n+1,s'} \langle c^\dagger_{n+1,s'} c_{n,s} \rangle - \langle c^\dagger_{n,s} c_{n+1,s'} \rangle \langle c^\dagger_{n+1,s'} c_{n,s} \rangle)].\end{aligned} \tag{2.6}$$

Then equation (2.2) is transformed into

$$\begin{aligned} H^{\text{HF}}_{\text{chain}} = &- \sum_{n,s} [t_0 - \alpha(u_{n+1} - u_n)](c^\dagger_{n+1,s} c_{n,s} + \text{HC}) \\ &+ U \sum_n \Big(\sum_s \rho_{n,-s} c^\dagger_{n,s} c_{n,s} - \rho_{n,\uparrow} \rho_{n,\downarrow} \Big) \\ &+ V \sum_{n,s} \Big[\sum_{s'} (\rho_{n-1,s'} + \rho_{n+1,s'}) c^\dagger_{n,s} c_{n,s} - \rho_{n,s} \sum_{s'} \rho_{n+1,s'} \Big] \\ &+ V \sum_{n,s} [-\tau_{n,s}(c^\dagger_{n,s} c_{n+1,s} + c^\dagger_{n+1,s} c_{n,s}) + \tau^2_{n,s}] \\ &+ \tfrac{1}{2} K \sum_n (u_{n+1} - u_n)^2 \end{aligned} \tag{2.7}$$

where $\rho_{n,s} = \langle c^{\dagger}_{n,s} c_{n,s} \rangle$ is the electron density, and $\tau_{n,s} = \langle c^{\dagger}_{n,s} c_{n+1,s} \rangle = \langle c^{\dagger}_{n+1,s} c_{n,s} \rangle$ is the bond order parameter.

Electronic systems are determined by the eigenvalue relation

$$\varepsilon_{\kappa,s}\varphi_{\kappa,s}(n) = -(t_0 - \alpha y_{n-1} + V\tau_{n-1,s})\varphi_{\kappa,s}(n-1) - (t_0 - \alpha y_n + V\tau_{n,s})\varphi_{\kappa,s}(n+1) + [U\rho_{n,-s} + V\sum_{s'}(\rho_{n-1,s'} + \rho_{n+1,s'})]\varphi_{\kappa,s}(n) + V_n\varphi_{\kappa,s}(n) \tag{2.8}$$

where $y_n = u_{n+1} - u_n$ is the bond variable, $\varepsilon_{\kappa,s}$ is the κth eigenvalue with spin s, and $\varphi_{\kappa,s}(n)$ the corresponding eigenfunction that satisfies the periodic boundary condition $\varphi_{\kappa,s}(n+N) = \varphi_{\kappa,s}(n)$. The lattice system is determined by the self-consistency condition

$$y_n = -\frac{2\alpha}{K}\sum_{\kappa,s}{}' \varphi_{\kappa,s}(n+1)\varphi_{\kappa,s}(n) + \frac{2\alpha}{KN}\sum_{m}\sum_{\kappa,s}{}' \varphi_{\kappa,s}(m+1)\varphi_{\kappa,s}(m) \tag{2.9}$$

where the prime indicates the sum over occupied states and the second term in (2.9) originates from the condition $\Sigma_n y_n = 0$ due to the periodic boundary condition: $u_{n+N} = u_n$.

Definitions of $\rho_{n,s}$ and $\tau_{n,s}$ are used as self-consistency equations:

$$\rho_{n,s} = \sum_{\kappa}{}' \varphi^2_{\kappa,s}(n) \tag{2.10}$$

and

$$\tau_{n,s} = \sum_{\kappa}{}' \varphi_{\kappa,s}(n)\varphi_{\kappa,s}(n+1). \tag{2.11}$$

When the set of wave functions $\{\varphi_{\kappa,s}(n)\}$, Hartree–Fock order parameters $\{\rho_{n,s}\}$, $\{\tau_{n,s}\}$, and dimerization order parameters $\{y_n\}$ are given, the total energy $E(\{x_i\})$ is calculated as a function of the dopant positions $\{x_i\}$. It is given by

$$E(\{x_i\}) = \sum_{\kappa,s}{}' \varepsilon_{\kappa,s} - U\sum_{n}\rho_{n,\uparrow}\rho_{n,\downarrow} - V\sum_{n}\left(\sum_{s}\rho_{n,s}\right)\left(\sum_{s'}\rho_{n+1,s'}\right) + V\sum_{n,s}\tau^2_{n,s} + \tfrac{1}{2}K\sum_{n}y_n^2 + \sum_{i\neq j}e^2/\varepsilon_{\perp}|x_i - x_j|. \tag{2.12}$$

The numerical method which determines $\{\varphi_{\kappa,s}(n)\}$, $\{\rho_{n,s}\}$, $\{\tau_{n,s}\}$, $\{y_n\}$ and $\{x_i\}$ is as follows.

(i) We assume that initial impurity positions $\{x_i^{(0)}\}$ are given.

(ii) The sets $\{\varphi_{\kappa,s}(n)\}$, $\{\rho_{n,s}\}$, $\{\tau_{n,s}\}$ and $\{y_n\}$ are determined self-consistently by (2.8), (2.9), (2.10) and (2.11). The method is the same as in [7–9].

(iii) The total energy $E(\{x_i\})$ is calculated by (2.12). With the help of the numerical sub-routine, the function $E(\{x_i\})$ is minimized and the set $\{x_i\}$ is determined. In the sub-routine, when $\{x_i\}$ is changed, the process (ii) is iteratively used to obtain a stationary value for $E(\{x_i\})$.

(iv) The set $\{x_i\}$, thus determined, may correspond to a local minimum of the energy $E(\{x_i\})$. We arbitrarily vary the initial set $\{x_i^{(0)}\}$, and perform the processes (i)–(iii).

Finally, we obtain $\{x_i\}$ that gives the minimum of $E(\{x_i\})$, by comparing the local minima obtained.

3. Stationary configurations

In the numerical work, the following values (SSH values) are used for the parameters: $\alpha = 4.1\,\text{eV Å}^{-1}$, $K = 21\,\text{eV Å}^{-2}$, and $t_0 = 2.5\,\text{eV}$. These give the dimensionless electron–phonon coupling constant $\lambda \equiv 2\alpha^2/\pi K t_0 = 0.20$. The short-range Coulomb strengths U and V are varied within $0 \leqslant U \leqslant 2.0\,t_0$ and $0 \leqslant V \leqslant 1.0\,t_0$. We investigate the effects of inter-impurity interactions by varying the interaction parameters generally. The magnitude of the Peierls gap may not agree with that of real samples. We, however, expect that general properties persist in realistic Peierls systems, as far as the Coulomb strengths are so weak that the mean-field approximation is applied successfully. The large coherence length of magnitude, nearly ten lattice constants, might also indicate validity of the mean field approximation for the short-range interactions. For the dopant potential, the parameters are $e^2 = 14.3\,\text{eV Å}^{-2}$, $\varepsilon_\perp = 2.5$, $\varepsilon_\parallel = 11.5$, $a = 1.22$ Å, and $d = 2.4$ Å. These were used by Conwell and Jeyadev [13]. The magnitudes of the dielectric constants are comparable to values observed experimentally over the whole sample. The system size is $N = 100$. As we consider the case with two acceptor ions, the electron number is $N_{\text{el}} = N - 2$.

Depending on the initial set $\{x_i^{(0)}\}$, two types of solutions are obtained. In the first type, two impurities are clustered as found in [11]. This solution is obtained from the initial value $|x_1^{(0)} - x_2^{(0)}|$ which is much smaller than $Na/2$. In the second type, the impurities are separated from each other. This type is obtained from $|x_1^{(0)} - x_2^{(0)}| \sim Na/2$. As the total energy of the second type is much larger than that of the first type (the difference is a few eV), we mainly report on the first type of solutions.

In figure 1, the relative impurity separation $\Delta x \equiv |x_1 - x_2|$ in the stable solutions is plotted by open squares as a function of U and V. In figures 1(a) and (b), results are shown for $U = 0$ and $1.0\,t_0$, respectively. Figures 1(c) and (d), results are depicted for $V = 0$ and $0.5\,t_0$, respectively. When U is kept constant and V increases, Δx also increases. Near a certain V ($V = 0.6\,t_0$ for figure 1(a) and $V = 1.0\,t_0$ for figure 1(b)), Δx suddenly increases and a phase transition occurs. When V increases further, the ground state of the system changes into a charge density wave state and Δx decreases. Hereafter, we limit our discussion to the system with the bond-order-wave ground state, because the latter are believed to be real systems. If V is taken as constant and U is varied, Δx does not change so much, as shown in figures 1(c) and (d).

In figure 2, a typical solution is depicted. The parameters are $U = 1.0\,t_0$ and $V = 0.5\,t_0$. Overall features do not change for other parameters as far as the ground state is in the bond-order-wave state. In figure 2(a), the smoothed bond variable, $\bar{y} \equiv \frac{1}{2}(-1)^n(y_n - y_{n+1})$, is shown. Centres of impurities are denoted by arrows on the abscissa. There is a polaron-like distortion around impurities. In figure 2(b), the smoothed electron density, $\bar{\rho}_n \equiv \frac{1}{4}(\rho_{n-1,s} + 2\rho_{n,s} + \rho_{n+1,s})$, is depicted. It does not depend on spin. We suppress the suffix s. The overall distribution is determined by the dopant potential as discussed in [9], it does not depend on spin. Reduced electron density is accumulated around the impurities. The total number of the reduction is two. In the impurity-free system with $U = V = 0$, we might obtain two charged solitons which are widely separated. In figure 2, they would be pinned by dopants. Thus, lattice distortion in figure 2(a) is not associated with a polaron but with a bipolaron trapped by the dopants.

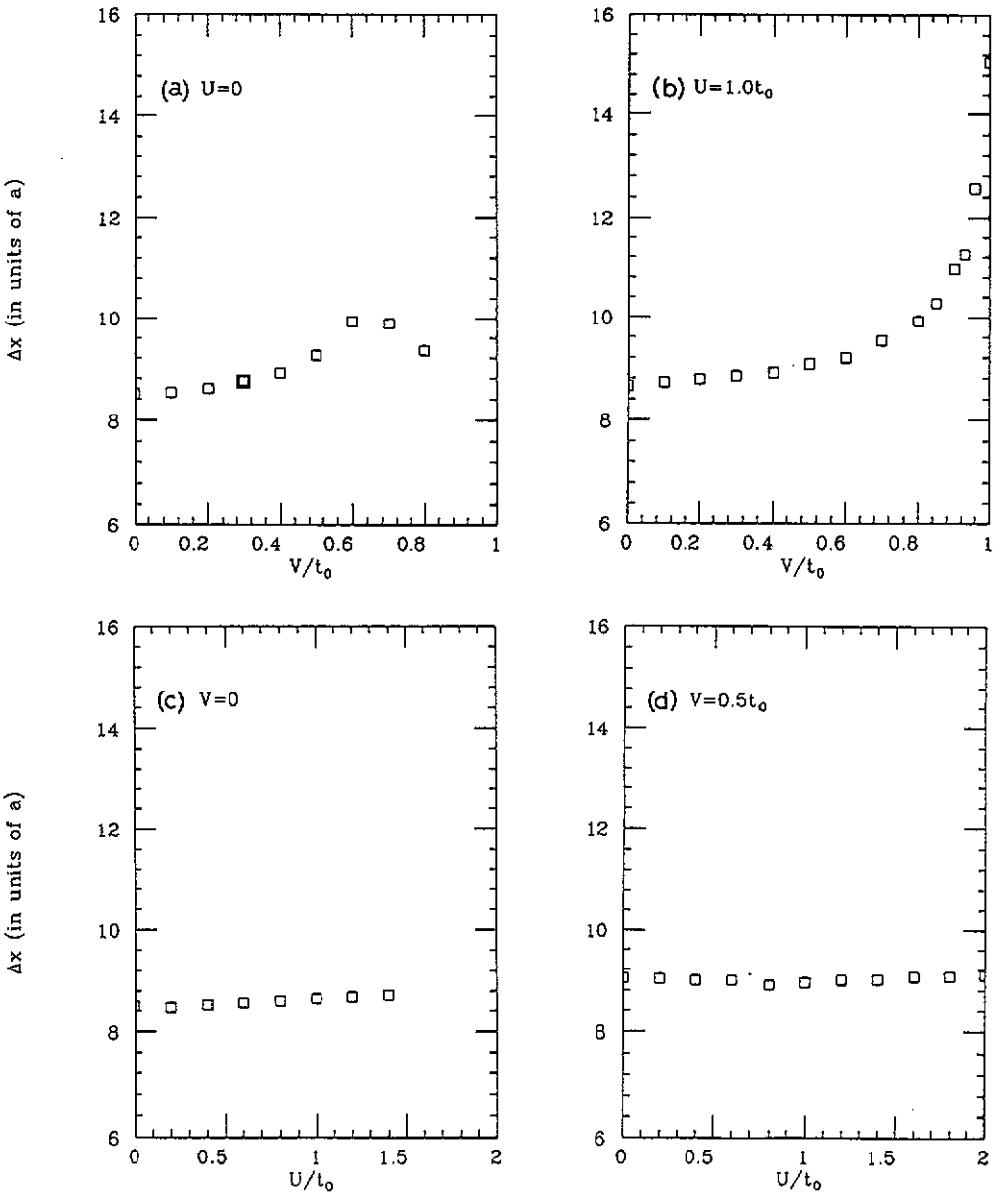

Figure 1. Inter-impurity separation Δx as a function of Coulomb repulsion strengths, U and V. The squares are the stable solutions.

In figure 2(c), the smoothed bond order parameter, $\bar{\tau}_n \equiv \frac{1}{4}(-1)^n(\tau_{n-1,s} - 2\tau_{n,s} + \tau_{n+1,s})$, is shown. Again, results do not depend on spin and the suffix s is suppressed. Spatial variation is similar to that of figure 2(a).

A trapped bipolaron is formed by competition among attractive forces between dopants and solitons and repulsive forces between solitons and also between dopants. The attractive force between a dopant and its adjacent soliton is always effective but

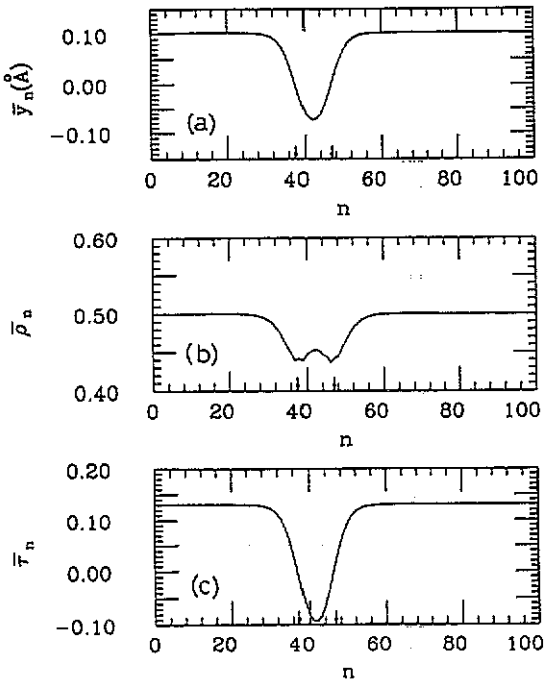

Figure 2. A typical stationary configuration. The parameters are $U = 1.0\,t_0$ and $V = 0.5\,t_0$. Centres of impurities are shown by arrows on the abscissa. Figure (*a*) is the smoothed dimerization amplitude, $\bar{y}_n = (-1)^n(y_n - y_{n+1})/2$, (*b*) is the smoothed electron density, $\bar{\rho}_n = \frac{1}{4}(\rho_{n-1,s} + 2\rho_{n,s} + \rho_{n+1,s})/4$ and (*c*) is the smoothed bond order parameter, $\bar{\tau}_n = (-1)^n(\tau_{n-1,s} - 2\tau_{n,s} + \tau_{n+1,s})/4$.

attraction between dopants and non-adjacent solitons is effective only when the distance between them is less than the coherence length. Then, the two solitons can be bound with the relative distance less than the coherence length. On the other hand, the repulsive force between solitons operates when the distance is shorter than the coherence length. Repulsion between dopants is stronger also. Two solitons thus cannot approach within much less than the coherence length. Consequently, the inter-soliton distance is of the order of the coherence length as shown in figure 1. The balance among the attractive and repulsive forces results in the formation of a trapped bipolaron state.

4. Energy level structure and dynamical conductivity

In figure 3, eigenvalues around the energy gap are plotted as a function of U and V. The broken line indicates the Fermi energy. The position is defined as an average of the highest occupied state and the lowest unoccupied state. Eigenvalues below the line are those of the occupied states and those above the line are of the unoccupied states. In a bipolaron in the impurity-free system, there are two localized energy levels in the gap, which are located symmetrically with respect to the gap centre [10]. They are unoccupied states. However, very different level structures are seen in figure 3. Two unoccupied localized states are shifted upward due to the positive dopant potential and there is a wide Peierls gap around the Fermi energy. The similar effect due to the strong dopant potential was obtained by Takahashi and Fukutome [15].

Next, we look at details of the level structures. In figure 3(*a*) for $U = 0$, a level splits off from the valence band for small V. As V increases, the splitting becomes smaller with a widening energy gap. At the transition to the charge density wave state, the splitting is suppressed. In figure 3(*b*) for $U = 1.0\,t_0$, a similar effect is observed. Furthermore,

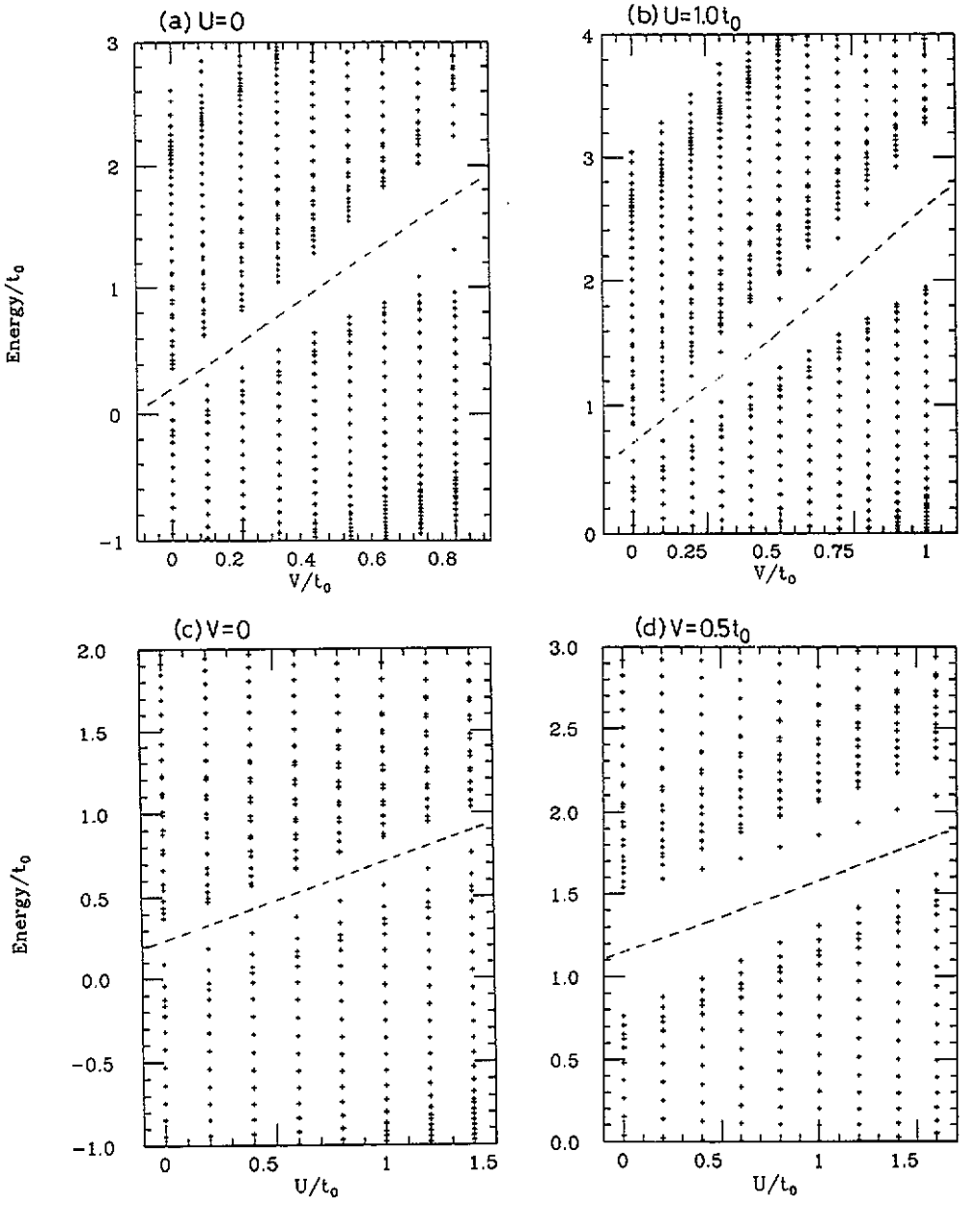

Figure 3. Eigenvalues around the energy gap as a function of U and V. The broken line indicates the Fermi energy.

another level splits down from the conduction band as V increases. In figure 3(c) for $V = 0$, there is a localized level split off upward from the valence band. This level is already depicted in figures 3(a) and (b) when $V = 0$. The width of the energy gap is almost constant. Figure 3(d) shows the case for $V = 0.5\,t_0$. As U increases, a new level splits down from the conduction band. This level has been already found in figure 3(b) when $U = 1.0\,t_0$ and $V = 0.5\,t_0$.

The following discussion is qualitative. One of the origins of the shift of the localized levels might be that U and V terms effectively give rise to a negative on-site potential around the solitons as seen in the third term on the right-hand side of (2.8). The negative potential is associated with the charge reduction around the dopants. This term moves the levels downward as U or V increases. In other words, the third term of (2.8) effectively weakens the strength of the dopant potential. The other origin might be that the order parameter increases as V increases. This prevents the levels from intruding into the conduction band as seen in figures 3(a) and (b).

In view of the new electronic structures shown in figure 3, it would be interesting to investigate the dynamical properties of the system. Here, we calculate the dynamical conductivity (optical absorption). The current operator is defined by

$$j_n = \mathrm{i}at_0 \sum_s (c^\dagger_{n+1,s}c_{n,s} - c^\dagger_{n,s}c_{n+1,s}). \tag{4.1}$$

We use the Kubo formula for the conductivity

$$\sigma(\omega) = \mathrm{i}\int_{-\infty}^{0} \mathrm{d}t\, \langle [j(0,t), j(0,0)]\rangle \frac{\mathrm{e}^{\mathrm{i}\omega t}}{\mathrm{i}\omega} \tag{4.2}$$

where

$$j(k,t) = \frac{1}{N}\sum_n \mathrm{e}^{-\mathrm{i}kna} j_n(t) \tag{4.3}$$

and

$$j_n(t) = \mathrm{e}^{\mathrm{i}Ht} j_n\, \mathrm{e}^{-\mathrm{i}Ht}. \tag{4.4}$$

Inserting (4.3) into (4.2), we get

$$\sigma(\omega) = \mathrm{i}(at_0)^2 \sum_s \sum_\kappa {\sum_\lambda}'' \frac{1}{\omega}\left(\frac{1}{\omega + \varepsilon_{\lambda,s} - \varepsilon_{\kappa,s} - \mathrm{i}\delta} - \frac{1}{\omega + \varepsilon_{\kappa,s} - \varepsilon_{\lambda,s} - \mathrm{i}\delta}\right) M^2_{\kappa,\lambda,s} \tag{4.5}$$

where

$$M_{\kappa,\lambda,s} \equiv \frac{1}{N}\sum_n [\varphi_{\kappa,s}(n)\varphi_{\lambda,s}(n+1) - \varphi_{\lambda,s}(n)\varphi_{\kappa,s}(n+1)] \tag{4.6}$$

and the prime and double-prime indicate the sum over the occupied and unoccupied states, respectively. The quantity δ is a positive infinitesimal. We replace δ with a finite quantity Δ in order to remove the finite size effect due to the sparse distribution of $\{\varepsilon_{\kappa,s}\}$. Then we get

$$\mathrm{Re}\,\sigma(\omega) = (at_0)^2 \sum_s {\sum_\kappa}' {\sum_\lambda}'' \frac{1}{\omega}\mathrm{Im}\left(\frac{1}{\omega + \varepsilon_{\kappa,s} - \varepsilon_{\lambda,s} - \mathrm{i}\Delta} - \frac{1}{\omega + \varepsilon_{\lambda,s} - \varepsilon_{\kappa,s} - \mathrm{i}\Delta}\right) M^2_{\kappa,\lambda,s}. \tag{4.7}$$

In figure 4, we show numerical results for the conductivity calculated by (4.7). We use $\Delta = 4t_0/N$. The magnitude of Δ is comparable to that of the mean level spacing of entire energy bands. The peak due to transition between valence and conduction bands looks continuous by the broadening parameter Δ. The optical absorption due to the presence of the localized level in the gap also broadens into a Lorentzian shape. Figures

4(*a–d*) correspond to the electronic structures depicted in figures 3(*a–d*), respectively. At a lower frequency region than the energy with respect to the inter-band-transition peak, a localized peak is found. It is obviously associated with the localized level in the energy gap discussed in figure 3. In figures 4(*a*) and (*b*), the positions of peaks move in the high-frequency direction as V increases. This is because the Peierls gap widens as V increases. In figures 4(*c*) and (*d*), the position of the largest peak does not change so much. This is due to the constant energy gap. The small peak of figure 4(*c*) moves only weakly as U changes. This is associated with figure 3(*c*). The localized level at the top of the valence band shifts slightly. The small peak in figure 4(*d*) moves to a lower frequency as U increases. It is also related to the change of the position of the localized level. Actually, in figure 3(*d*), the localized level below the conduction band intrudes into the energy gap. In these ways, the dynamical conductivity reflects the changes in electronic structures.

5. Summary and discussions

In this paper, we have discussed how the inter-impurity interactions alter the dopant configuration, lattice pattern, and energy level structures. The study has been confined to the system with two dopants. We find trapping of a bipolaron around the dopants. The distance between two solitons is of the order of the coherence length. This is due to the balance between the attractive and repulsive forces among dopants and solitons in the chain. Electronic level structures are modified due to the strong dopant potential. Two mid-gap levels, which exist in a free bipolaron, are absorbed by the conduction band. A similar effect was obtained by Takahashi and Fukutome [15]. We find that the Coulomb interactions in the chain effectively weaken the strength of the dopant potential. This effect explains well the change of the level structure as a function of the Coulomb strength in the chain. A new level is emitted from the conduction band or the localized level in the gap comes closer to the valence band when the strength becomes large. The frequency dependence of the dynamical conductivity is related to the change of level structure. The position of the inter-band-transition peak shows the width of the energy gap. The isolated peak in the lower frequency range is associated with the position of the localized level in the energy gap.

To the best of our knowledge, experimental evidence of impurity clustering and existence of a trapped bipolaron has not yet been obtained. The reason might be that optical absorption data of doped conjugated polymers are very broad, and they are a mixture of absorption peaks originating from many types of solitonic excitations, such as, solitons, polarons, and bipolarons. It would be difficult to observe separately peaks due to a single solitonic excitation. Experiments with better resolution would be desirable.

In x-ray experiments, it is now established that chains and dopant columns are crystallinely ordered in the direction perpendicular to the chains. But peaks, which indicate ordering of dopants in the chain direction, seem to be absent in x-ray data (see, for example, figure 1(*b*) of [14]). When better data are obtained we will be able to determine whether impurity clustering occurs or not.

The number of impurities has been confined to two in this paper. We should investigate systems with more impurities. Preliminary calculations of systems with from three to five impurities show that there are various types of stationary solutions. For the three impurities, there are three types. In the first type, the three dopants cluster. In the

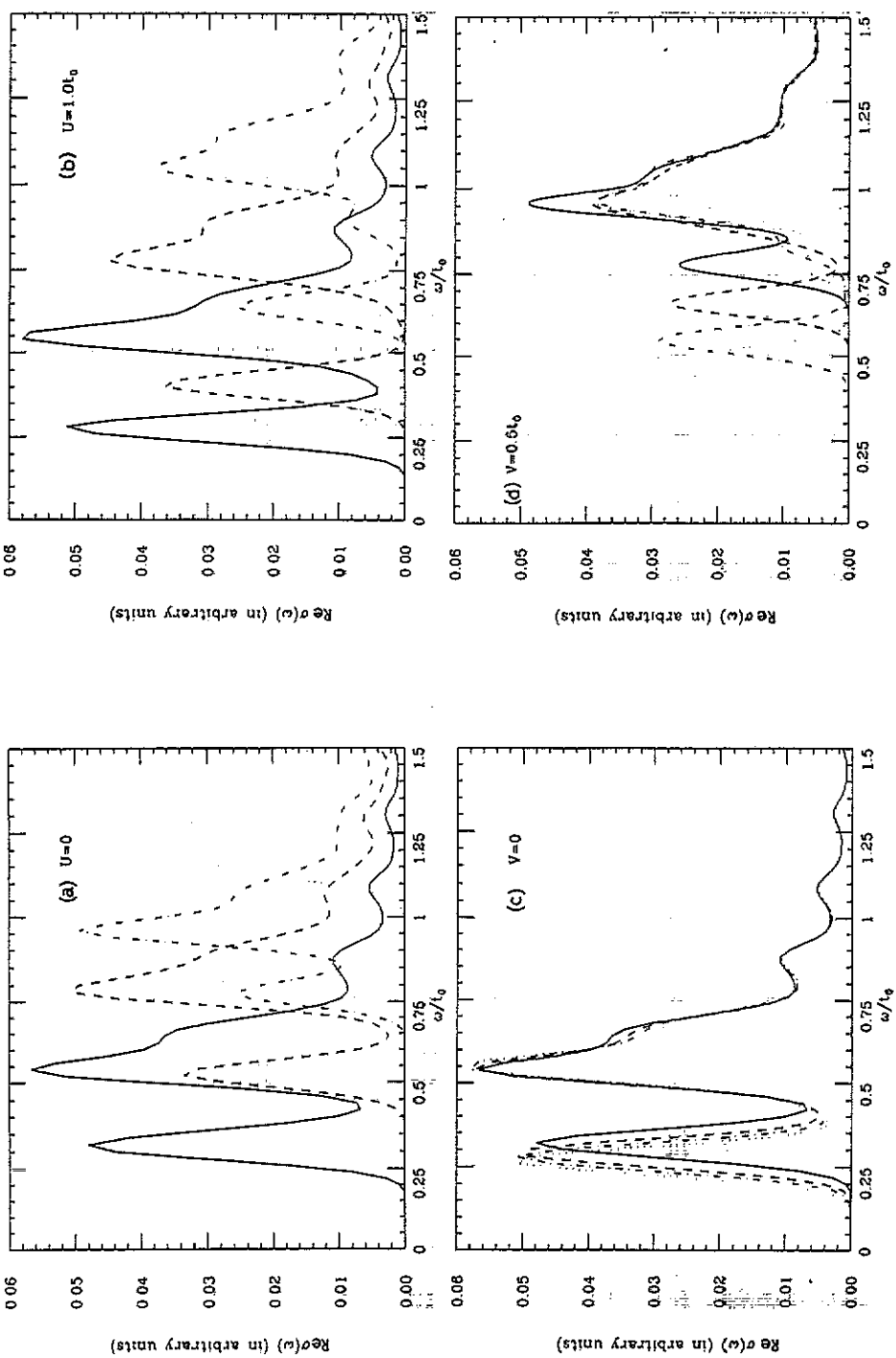

Figure 4. Dynamical conductivity as a function of U and V. The broadening parameter in equation (4.7) is $\Delta = 4\,t_0/N$. Figure (*a*) is for $U = 0$ with $V = 0$ (full line), $0.3\,t_0$ (broken line), $0.5\,t_0$ (chain line), and $0.7\,t_0$ (dotted line). (*b*) is for $U = 1.0\,t_0$ with $V = 0$ (full line), $0.3\,t_0$ (broken line), and $0.6\,t_0$ (chain line). (*c*) is for $V = 0$ with $U = 0$ (full line), $0.6\,t_0$ (broken line), $1.0\,t_0$ (chain line), and $1.4\,t_0$ (dotted line), and (*d*) is for $V = 0.5\,t_0$ with $U = 0$ (full line), $0.4\,t_0$ (broken line), $1.0\,t_0$ (chain line), and $1.6\,t_0$ (dotted line).

second, two dopants cluster and the other is isolated. In the third, the three dopants are mutually isolated. The total energy increases from the first to the third type. For more impurities than three, there exist many more types of solutions. For clustered impurities, the distance between the nearest-neighbour impurities is still of the order of the coherence length. The balance between the attractive and repulsive forces is also effective in systems with many impurities. This strongly implies that the inter-impurity interactions are the origin of the correlated distribution of impurities.

What we have to study in the next stage is how the above findings are related to the metal–insulator transition. As we have shown in [8, 9], the emergence of a density of states at the Fermi energy due to disorders is a powerful mechanism for the metallic behaviour. We can explain well the appearance of the Pauli susceptibility, its magnitude, and the critical concentration, observed in experiments. On the other hand, the metal–insulator transition is also observed in highly oriented samples [14]. Though the impurity distribution might be quite disordered in the chain direction, some correlation may exist between the dopants. Our present model enables us to treat the 'semi-random' distribution. A sample average over many metastable solutions with various types of stationary impurity configurations should be done. We would be able to obtain information on the density of states and clarify how the inter-impurity correlation effect the mechanism of the metal–insulator transition reported in previous papers [8, 9].

The three-dimensional effect is another interesting problem. We can perform further calculations by taking account of geometries about chains and dopant columns, which were proposed by the x-ray analysis [14]. Knowledge of the way the structure of a trapped bipolaron changes is of particular interest.

Acknowledgments

Fruitful discussions with Professor Y Wada, Dr K Yamaji and Dr A Terai are acknowledged. Numerical work has been carried out on the HITAC M-680 and S-820 of the Computer Center of the University of Tokyo, and also on the HITAC M-680 and S-820 of the Institute of Molecular Science, Okazaki National Research Institutes, Japan.

References

[1] Harigaya K, Wada Y and Fesser K 1989 *Phys. Rev. Lett.* **63** 2401
[2] Harigaya K, Wada Y and Fesser K 1990 *Phys. Rev.* B **42** 1268
[3] Harigaya K, Wada Y and Fesser K 1990 *Phys. Rev.* B **42** 1276
[4] Harigaya K 1990 *J. Phys. Soc. Japan* **59** 1348
[5] Harigaya K, Wada Y and Fesser K 1990 *Phys. Rev.* B **42** 11303
[6] Harigaya K, Wada Y and Fesser K 1990 *Strongly Coupled Plasma Physics* ed S Ichimaru (Amsterdam: Elsevier/Yamada Science Foundation) p 255
Harigaya K, Wada Y and Fesser K 1991 *Synth. Met.* **43** 3579
[7] Harigaya K, Terai A, Wada Y and Fesser K 1991 *Phys. Rev.* B **43** 4141
[8] Harigaya K and Terai A 1991 *Synth. Met.* **43** 3481; 1991 *Solid State Commun.* **78** 335
Harigaya K 1991 *Chem. Phys.* submitted
[9] Harigaya K and Terai A 1991 *Phys. Rev.* B **44** at press
[10] Heeger A J, Kivelson S, Schrieffer J R and Su W-P 1988 *Rev. Mod. Phys.* **60** 781
[11] Cohen R J and Glick A J 1989 *Phys. Rev.* B **40** 8010

[12] Su W-P, Schrieffer J R and Heeger A J 1980 *Phys. Rev.* B **22** 2099
[13] Conwell E M and Jeyadev S 1988 *Phys. Rev. Lett.* **61** 361
[14] Murthy N S, Shacklette L W and Baughman B H 1990 *Phys. Rev.* B **41** 4708
[15] Takahashi A and Fukutome H 1989 *Synth. Met.* **28** D469